JOURNAL OF MATERIALS SCIENCE **35** (2000) 4039–4047

The strain dependent indentation resilience of auxetic microporous polyethylene

K. L. ALDERSON*
Faculty of Technology, Bolton Institute of Higher Education, Deane Road, Bolton BL3 5AB, UK

A. FITZGERALD
Department of Materials Science and Engineering, University of Liverpool, PO Box 147, Liverpool L69 3BX, UK

K. E. EVANS
Department of Engineering, University of Exeter, North Park Road, Exeter EX4 4QF, UK

A series of tests have been conducted on (i) auxetic, (ii) compression moulded and (iii) sintered ultra high molecular weight polyethylene. The auxetic material possesses a negative Poisson's ratio, ν, due to its complex porous microstructure which consists of nodules interconnected by fibrils and the sintered material has a positive ν and is microporous but does not contain fibrils. It was found that the auxetic material was both more difficult to indent than the other materials at low loads (from 10–100 N) and was the least plastic with the most rapid viscoelastic creep recovery of any residual deformation. Indeed, at low loads, where the resistance to local indentation is most elastic, the hardness increased by up to a factor of 8 on changing the Poisson's ratio from $\nu \approx 0$ to $\nu \approx -0.8$. A mechanism is proposed based on local densification under the indentor of the nodules and fibrils which explains how the microstructural response of an auxetic polymer can be used to interpret the results.

1. Introduction

Although it is theoretically possible for both isotropic and anisotropic materials to possess a negative Poisson's ratio (ν), it is generally believed that nearly all materials, whether synthetic or naturally occurring, have a positive ν. However, in 1987 [1], a novel polymeric foam was fabricated that expanded both transversely to and along the direction of an applied tensile load i.e. it had a negative ν. This discovery has led to a range of materials being fabricated which also show this effect, including metallic foams [2], microporous polymers [3–5] and carbon fibre composite laminates [6]. These materials are now referred to as auxetic materials [7].

Apart from possessing the counter-intuitive Poisson's ratio effect, auxetic materials are interesting because, from classical elasticity theory, many of their properties (such as plane strain fracture toughness and shear modulus) are predicted to be enhanced [1, 8, 9]. One such property is the elastic indentation resistance, H_e, which is related to Poisson's ratio as:

$$H_e \propto (1 - \nu^2)^{-x} \tag{1}$$

where the value of x depends on the theoretical analysis used. For example, if a classical Hertzian model for two contacting spheres is adopted, x is 2/3 [10] whereas if the system is treated as a uniform pressure distribution over a circular cross-section on a semi-infinite solid, $x = 1$ [11]. For positive ν for a range $0 \leq \nu \leq 0.5$, the indentation resistance varies little. However, for isotropic materials with $-1 \leq \nu \leq 0$ being possible, the indentation resistance may increase greatly. This has been found to be the case i.e. enhancements are found in the indentation resistance of auxetic materials such as carbon fibre laminates [6], foams [12, 13] and polymers [14] due to their having a negative ν. Indeed, work done previously on comparing auxetic ultra high molecular weight polyethylene (UHMWPE) with compression moulded UHMWPE [14] has shown that the auxetic material is up to three times more difficult to indent than the conventional material at low loads. The load range investigated was 25–250 N.

In this paper, the elastic indentation behaviour of auxetic UHMWPE is further investigated in detail. Since auxetic behaviour is essentially an elastic phenomenon it may be expected that the maximum benefits occur when plasticity during indentation is at a minimum. Hence, the load range has been extended particularly at very low loads, with analysis beginning at a test load of 5 N. The elastic and plastic elements of the indentation response were also examined. During the indentation process, under the application of the load, the material undergoes both elastic and plastic deformation.

* Author to whom all correspondence should be addressed.

The plastic deformation results in the formation of a permanent impression while the stored elastic energy is released, once the load is removed [15]. In addition, the viscoelastic creep response to indentation was also investigated with the observation of the indented specimens over a period of up to a month.

2. Experimental

2.1. Specimen fabrication

The details on how the specimens for this work were fabricated have been well documented, particularly for the auxetic UHMWPE [16–18]. However, for completeness, they will be summarised below. In all cases, the UHMWPE powder used was GUR 415 supplied by Hoechst [19].

2.1.1. Fabrication of auxetic UHMWPE

Auxetic UHMWPE was produced by a three stage process based on the powder metallurgy techniques of compaction, sintering and extrusion. All the stages took place within a specially designed processing rig with a barrel of diameter 15 mm and length 165 mm. For the compaction stage, the barrel was blocked off using a blank die. The powder was introduced and was allowed to reach equilibrium at a temperature of 110°C for 10 minutes. Then, compaction commenced at a rate of 20 mm/min. and a compaction pressure of 0.04 GPa was held for 20 minutes, resulting in a rod with sufficient structural integrity to allow handling. The rod was removed from the rig and allowed to cool to room temperature.

The rod was re-introduced into the rig which was now at a temperature of 160°C so that the rod sat in the middle of the barrel i.e. not in contact with the extrusion die now fitted to the rig. This was to ensure the required amount of expansion during the sintering stage [17], which lasted for 20 minutes. Immediately after this, the extrusion plunger was driven into the barrel at a rate of 500 mm/min., forcing the UHMWPE through a conical die of entry diameter 15 mm, exit diameter 7.5 mm and cone semi-angle 30° followed by a capillary of length 3.4 mm and diameter 7.5 mm. The extrudate thus produced was smooth and continuous with cup-and-cone fractures restricted to the specimen ends.

2.1.2. Fabrication of sintered UHMWPE

This material was used as a direct comparison with the auxetic UHMWPE. Basically, it is a form of conventional UHMWPE with a positive ν but is microporous and has a density very similar to that of the auxetic UHMWPE. It was produced by following the first two stages of the process as described above i.e. by compaction and sintering alone. After sintering was complete, the rod thus fabricated was simply ejected from the barrel.

2.1.3. Fabrication of compression moulded UHMWPE

This material was used as a comparison with the auxetic and sintered forms of UHMWPE. In order to ensure that the highest quality of plaque could be produced, an extensive series of tests was carried out varying the temperature, pressure and time at pressure. The plaques thus produced were then assessed in terms of their mechanical properties and variation of these within each plaque and between plaques [20]. As a consequence of this, the following conditions were selected.

Preliminary room temperature pressing of the material was necessary to ensure that all the entrapped air (which could lead to air bubbles in the final product) was removed. After this preliminary treatment, the hydraulic press was heated to 165°C, the pretreated powder and mould were placed in it and a pressure of 11.5 MN/m^2 was applied for 15 minutes. After this, the moulded plaque was water cooled rapidly under the weight of the press. Once cooled, the plaque was removed from the mould and any excess polymer in the form of flash was trimmed.

2.2. Ball indentation

Indentation testing was carried out on the processed forms of UHMWPE. In order to perform the tests, a small amount of specimen preparation was required for the auxetic and sintered specimens. These are produced in the form of rods and were sectioned to produce flat bars of length 40 mm, width 10 mm and depth 3 mm (see Fig. 1). After this, the bars were ground slightly to reduce any surface defects. The moulded plaques required no additional specimen preparation. The load in all cases was applied in the radial, r, direction, as indicated in Fig. 1 as this is the direction in which the negative Poisson's ratio is found in the material due to the orientation of the microstructure.

In order to eliminate any relaxation effects which may result in inconsistencies and indeed in incorrect values of elastic indentation resistance being obtained, the tests were carried out so that the depth of penetration of the indentor was measured during load application [21]. This was measured by extensometry and plotted directly against the applied load.

The tests were performed by allowing a 5 mm diameter steel ball to penetrate into the test specimen

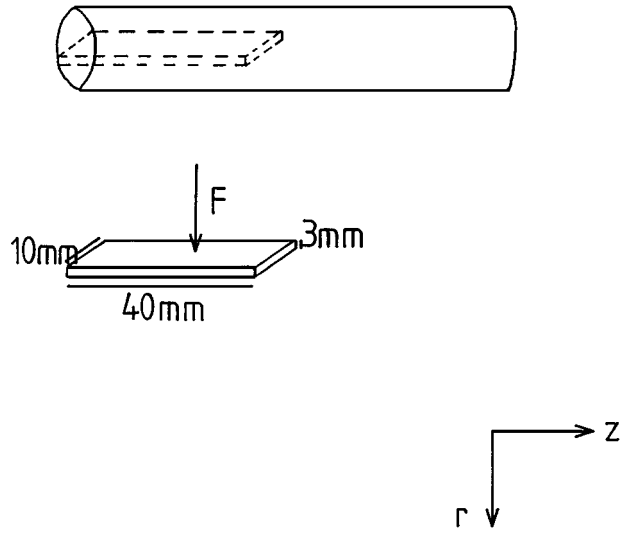

Figure 1 Schematic showing the radial, r, testing direction for the indentation tests.

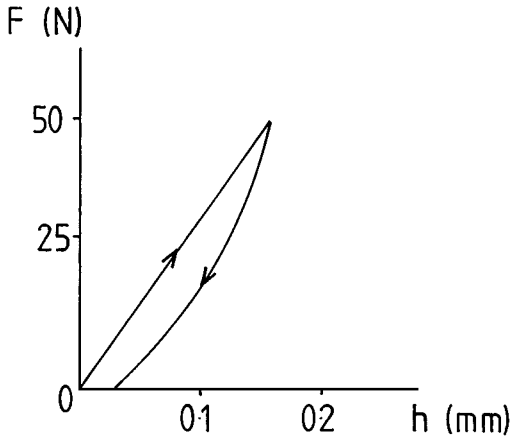

Figure 2 Typical graph of indentation load, F, against indentation depth, h.

until the required test load was achieved. In this case, the loads used were 15 N, 25 N, 50 N, 75 N, 100 N, 150 N, 200 N and 250 N. At each load, at least three specimens of each type of UHMWPE were tested. For all the specimens of all the different forms considered, the data were analysed as follows. For the test load of 15 N, analysis of the loading portion of the curve was also conducted at 5 N and 10 N. Likewise, for the test load of 25 N, analysis was also conducted at 5 N, 10 N and 20 N and for the test load of 50 N at 10 N and 25 N. For the remaining test loads (i.e. 75 N, 100 N, 150 N, 200 N and 250 N), analysis was carried out only at the peak applied load. The tests were carried out using an Instron 1185 mechanical testing machine with a crosshead speed of 0.5 mm/min. The full scale deflection was altered to give the clearest load/displacement plots as the test load was varied. Accuracy was ensured by re-calibration of the Instron between each test. An example of a typical load/displacement curve produced is shown in Fig. 2.

The loading portion of the curve was used to generate the elastic equivalent of the Brinell hardness number for the material, H_e, given by:

$$H_e = \frac{F}{\pi a^2} \tag{2}$$

where F is the applied force and a the radius of the area of contact. Assuming that indentation depth is small compared with the ball radius, then:

$$a^2 \approx 2Rh \tag{3}$$

where R is the radius of the indentor and h the indentation depth. Thus,

$$H_e = \frac{F}{2\pi Rh} \tag{4}$$

Once the test load had been applied, as can be seen from Fig. 2, the load was then removed immediately at the same rate so that the unloading characteristics and the amount of retained deformation could be studied without any residence time. The retained deformation was recorded at the end of the test and again after 1 month.

2.3. Measurement of Poisson's ratio

So that the relationship between the elastic indentation resistance of the materials fabricated and tested and their Poisson's ratios can be evaluated, it is necessary to measure the Poisson's ratio of the actual material tested. This was carried out for the sintered material and the compression moulded plaques without much difficulty. The specimens were subjected to simple compression testing in the radial (r) direction and these were monitored using a photographic technique developed in-house. This allowed for accurate measurements of the strains to be made. However, it should be noted that the strains thus measured are engineering strains and the resulting strain ratio is only, strictly speaking, the Poisson's ratio for small linear elastic strains [22]. In this case, the measured values obtained are, for the sintered material, $\nu = +0.11$ and for the compression moulded plaques, $\nu = +0.20$.

However, it is well documented that auxetic materials may exhibit strain dependent behaviour. Thus a more complex analysis method must be employed for these materials. This approach has been previously used very effectively to analyse the experimental data gathered from indentation testing of auxetic UHMWPE [14] and so will be employed here. In order to conduct such analysis, however, data from more than 100 separate compression tests were gathered. Small sections of auxetic rods were subjected to simple compression testing in the radial (r) direction as for the sintered material and the compression moulded plaques and monitoring took place using the in-house photographic technique, allowing the engineering strains to be very accurately obtained and the total engineering strain ratio in the radial direction, N_{rz}, to be calculated from:

$$N_{rz} = \frac{-e_z}{e_r} \tag{5}$$

where e_r and e_z are the engineering strains in the r and z directions and the load is applied in the r direction (see Fig. 1). This experimental total engineering strain ratio was then used to calculate the Poisson's ratio. The details of the analysis method are given fully in section 3 below.

A further consequence of the strain dependent nature of the behaviour of auxetic materials is that the actual values of Poisson's ratios obtained by analysis cannot be used as they are. This is because these values of ν are obtained at a certain strain which is not usually that at which the ball indentation tests are carried out. Thus, further data manipulation is required at this stage [14], which is also detailed in section 3.

2.4. Microscopic examination of auxetic UHMWPE

Samples of the auxetic UHMWPE extrudates were taken, mounted on aluminium stubs, sputter coated with gold and observed in a Philips 501 SEM at magnifications of up to $\times 1250$. The purpose of this was two-fold. The microstructure which produces the negative ν effect is well documented for polymeric materials as being nodules interconnected by fibrils and observation of

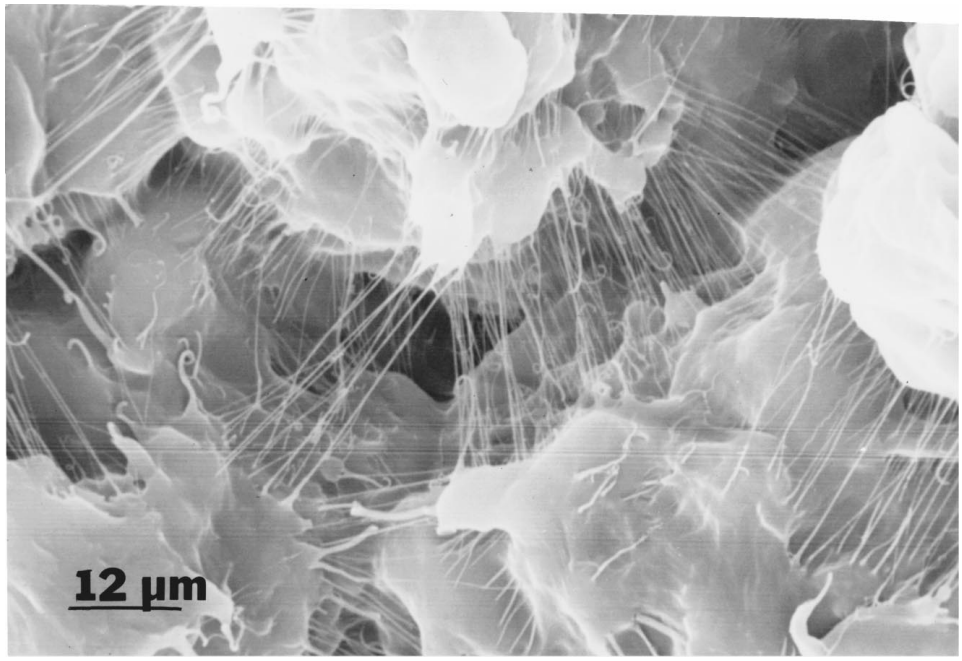

(a)

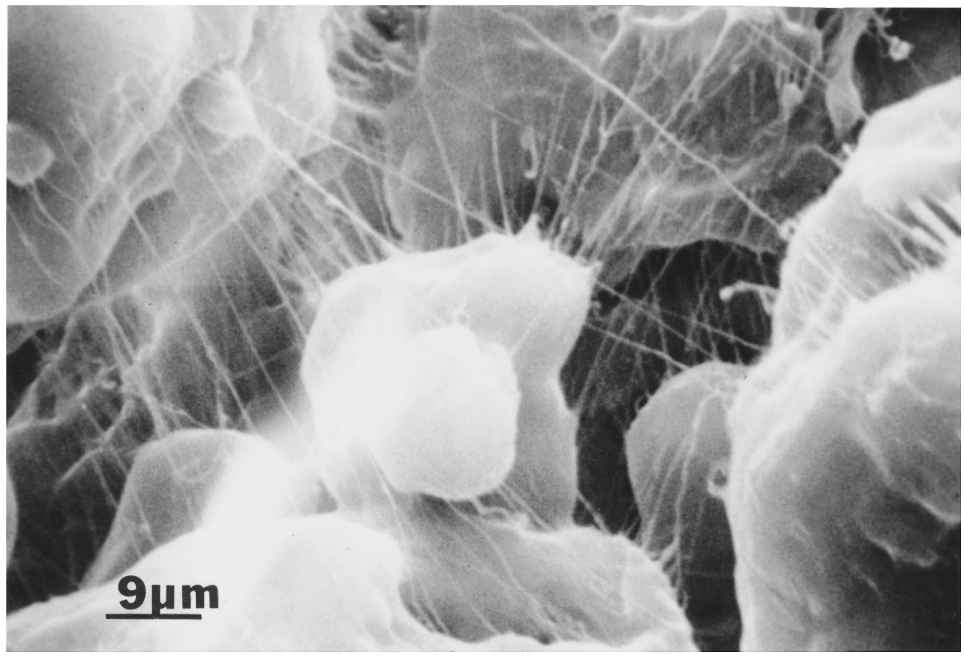

(b)

Figure 3 Two examples of the microstructure of auxetic UHMWPE, each displaying a range of fibril angles.

the samples in this work allowed conformation of this microstructure. Fig. 3a and b show typical examples of the microstructure of auxetic UHMWPE specimens used in this work and Fig. 4 is a general schematic of the microstructure of auxetic polymers. Secondly, it was necessary for the data manipulation required here for the size, shape and orientation of the microstructural parameters shown schematically in Fig. 4 to be measured. (The shaded rectangles represent the nodules of sides a and b and the solid lines the interconnecting fibrils of length l, as labelled in Fig. 4. There is no material in the unshaded regions.) To achieve this, photographs of the microstructure of a large number of specimens were taken and from these, measurements of the nodule and fibril dimensions were made. In addition, α, the angle between the fibril and the r axis, was monitored.

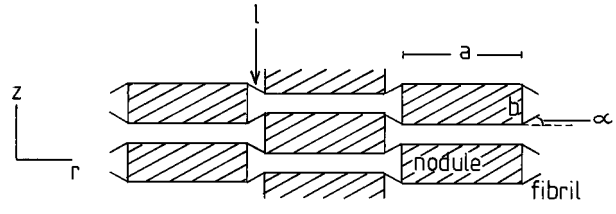

Figure 4 Schematic of the microstructure of an auxetic polymer, showing the parameters a and b (the major and minor lengths of the nodules, represented by the shaded rectangles), l (the fibril length) and α (the angle between the fibril and the r axis).

3. Use of nodule-fibril geometric models to aid in indentation analysis

The analysis used for the complete interpretation of the indentation data involves three stages, which are considered below.

Firstly, the results from the experimental compression tests were plotted to produce the total engineering strain ratio against strain plots. Due to the nature of the material produced, the microstructure can be variable and thus, in order to interpret fully the graphs, it is necessary to find the best fit model curves to the experimental single test data. This is achieved using models based on the geometry of Fig. 4, in this case giving:

$$N_{rz} = -\frac{(\sin\alpha_0 - \sin\alpha)(a + l\cos\alpha_0)}{(\cos\alpha - \cos\alpha_0)(b - l\sin\alpha_0)} \qquad (6)$$

where α_0 is the initial fibril angle to the r axis before any loading takes place, l is the fibril length and a and b are the major and minor lengths of the rectangular nodules [22]. From SEM examination, $a/b = 0.9$ and

$$l = 0.05a \qquad (7)$$

but the initial fibril angle was found to vary greatly. It was this quantity which was used as an adjustable parameter to obtain the best possible agreement of the model with the experimental results. To interpret the data correctly, then, it is necessary to see if certain discrete values of α_0 can be identified or if a summation average for N_{rz} should be used. It was found that though a range of angles was represented in the specimens, the majority of data points fell close to model values obtained using $\alpha_0 = 20^\circ$, $\alpha_0 = 50^\circ$, $\alpha_0 = -20^\circ$ and $\alpha_0 = -50^\circ$ (see Fig. 5 for these plots). As already stated, in excess of 100 compression tests were carried out to obtain these data. So, for clarity, the large number of data points are omitted from Fig. 5, which simply shows the four lines generated by Equation 6 to represent most closely the experimental data points. This degree of variation of the microstructure is as expected since it is known that a large degree of anisotropy exists and the values of α_0 quoted are seen in SEM examinations of auxetic UHMWPE. The significance of the latter two angles has been previously discussed with reference to auxetic polypropylene [5]. The minus

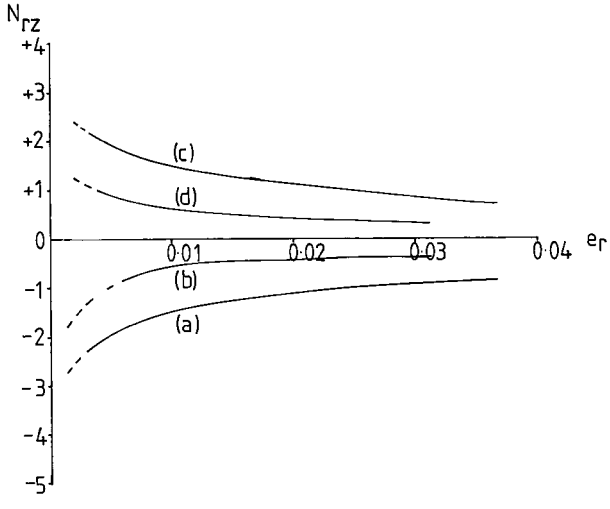

Figure 5 Graph of total engineering strain ratio, N_{rz}, against strain (e_r) for auxetic UHMWPE. (a) represents a best fit line with $\alpha_0 = 20^\circ$, (b) has $\alpha_0 = 50^\circ$, (c) has $\alpha_0 = -20^\circ$ and (d) has $\alpha_0 = -50^\circ$. Data points are omitted for clarity.

sign indicates that the microstructure is over-expanded and the result of this is strain dependent but positive ν behaviour as opposed to auxetic behaviour. This can be just as beneficial for enhancements in indentation resistance, as the latter varies as ν^2 of course. The engineering strain in the radial direction, e_r, based on the geometry of Fig. 4, is given by (see [22] for details):

$$e_r = \frac{l(\cos\alpha - \cos\alpha_0)}{a + l\cos\alpha_0} \qquad (8)$$

The second stage of the analysis was to use the calculated and experimentally verified engineering strain ratio against strain plot to obtain a theoretical Poisson's ratio against strain plot. This was achieved by using the experimentally obtained values of a, b and l in conjunction with the best fit values of α_0. These parameters were fed into the nodule-fibril model for Poisson's ratio ν_{rz}, where the load is applied in the r direction, which is:

$$\nu_{rz} = -\frac{(\cos\alpha)(a + l\cos\alpha)}{(\sin\alpha)(b - l\sin\alpha)} \qquad (9)$$

The derivations of Equations 7–9 are given in full in a previous publication [22].

The theoretically determined plot of ν against e can now be used to generate the required Poisson's ratio associated with the strain incurred by each individual elastic indentation test. The average strain experienced by the material during the test was calculated using an empirical formula proposed by Tabor [23]:

$$e \approx 0.2\left(\frac{a}{R}\right) \qquad (10)$$

Assuming small indentation depths,

$$e = 0.2\left(\frac{2h}{R}\right)^{1/2} \qquad (11)$$

$$= 0.4\left(\frac{h}{D}\right)^{1/2} \qquad (12)$$

where D is the diameter of the indenter. The constant 0.2 was used by Tabor to indicate plastic strain. In this work, particularly at low strains, the indentation process is mainly elastic rather than plastic, so here, the strain was estimated using:

$$e = 0.2\left(\frac{h}{D}\right)^{1/2} \qquad (13)$$

This somewhat arbitary choice has been previously employed and shown to be an accurate approximation [14]. For each indentation test, a value of strain was calculated using Equation 13 and the corresponding value of ν_{rz} for each strain was obtained by reading the values off the theoretically determined but experimentally based plot of ν_{rz} against strain. This allowed a ν_{rz} associated with each value of H_e to be identified.

4. Results

4.1. Variation of indentation resistance with Poisson's ratio

Table I gives the values of indentation resistance of the three differently processed forms of UHMWPE. For the sintered and compression moulded materials, the indentation resistance quoted is a simple average. For the auxetic material, however, the average indentation resistance is not a meaningful quantity due to the strain dependency of the material. So, here, the range of values attained is given. A better representation of this is shown in Fig. 6 which plots the indentation resistance against Poisson's ratio for selected test loads of 10 N, 15 N, 50 N and 100 N for the auxetic, sintered and compression moulded materials. Similar plots were obtained for the remaining loads investigated up to 100 N. Note that the error bars have been omitted from the compression moulded data in Fig. 6 for clarity, but these are given in Table I.

It can be seen from Table I and Fig. 6 that enhancements are found in indentation resistance due to the material being auxetic at loads from 10 N upwards. Enhancements were not found at the lowest investigated load of 5 N. This could be due to the very small load involved i.e. to inaccuracies in the test method at low loads and strains or it could be due to the way in which the material responds initially to indentation. The indentation resistance values for the compression moulded and sintered materials are very similar from 15 N to 100 N, with the auxetic UHMWPE being substantially more difficult to indent in this load range i.e. up to about twice the values at 15 N and 25 N. Here, for 15 N, the average indentation resistance of the sintered and compression moulded material is 10 N/mm^2 with the auxetic material having values of indentation resistance increasing up to 18 N/mm^2 and for 25 N, the average indentation resistance of the sintered and compression moulded material is 13 N/mm^2 with the auxetic material having values of indentation resistance increasing up to 23 N/mm^2.

After 100 N, the auxeticity of the material is lost, i.e. $\nu = 0$ due to the higher strains being imposed. It is for this reason that in Table I, an average indentation resistance with standard deviation is quoted for the test loads of 150 N and 200 N for all three material types.

Fig. 7a shows the measured indentation resistance against Poisson's ratio at 25 N using the microstructural model with $a/b = 0.9$, $l = 0.05a$ and $\alpha_0 = 20^\circ$. a/b and l are obtained directly from SEM photographs while $\alpha_0 = 20^\circ$ provides the best fit as discussed previously. Also plotted on both Fig. 7a and b are the data points for the sintered and compression moulded materials at values of $\nu = +0.11$ and $\nu = +0.20$ respectively. By using the same values of a/b and l it was possible to fit all the data to one curve, using only 3 values of $\alpha_0 : 20^\circ$, 50° and -50°, the majority being fitted with $\alpha_0 = 20^\circ$. This is shown in Fig. 7b. This process was repeated for test loads of 5 N, 10 N and 15 N and similar results were obtained again using the same three initial angles with the same initial geometry. Basically, scatter in the test data could be eliminated by using one of the three identified initial angles in the analysis. This indicates once again the variabilty of the microstructure and also the importance of careful identification of the model parameters.

TABLE I Ball indentation resistance values of the sintered (S), compression moulded (CM) and auxetic materials (A). For both the former, an average value at each load is quoted; for the latter, the range of values attained is given

	Indentation resistance (N/mm^2)		
Test load (N)	CM	S	A
5	6 ± 3	3 ± 2	1 – 6
10	9 ± 4	6 ± 3	2 – 16
15	10 ± 4	10 ± 4	3 – 18
25	13 ± 5	13 ± 4	4 – 23
50	18 ± 5	19 ± 4	9 – 29
75	23 ± 5	23 ± 4	20 – 32
100	25 ± 5	27 ± 5	23 – 36
150	29 ± 5	33 ± 4	34 ± 3
200	30 ± 4	37 ± 3	37 ± 2

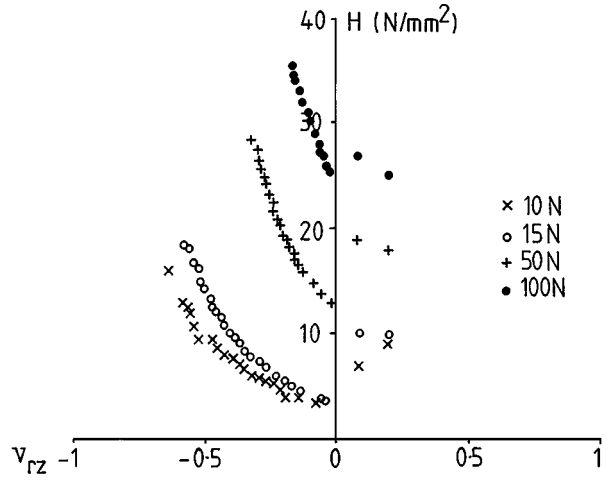

Figure 6 Graph of elastic indentation resistance (H_e) against Poisson's ratio (ν_{rz}) at test loads of 10 N, 15 N, 50 N and 100 N. For comparison, the sintered and compression moulded data are also plotted at each load.

4.2. Elastic and viscoelastic recovery of indentations

The values of the initial retained deformation expressed as a percentage of the total indentation depth, h, are shown in Table II for all three types of material. The data were gathered from at least three specimens tested at each load from 15 N to 250 N and the following can clearly be seen.

Firstly, the auxetic UHMWPE is the most elastic of the three materials tested at the lower loads (i.e. $5 \pm 2\%$ compared with $7 \pm 1\%$ for the compression moulded and $11 \pm 3\%$ for the sintered materials at 15 N and $8 \pm 2\%$ compared with $13 \pm 2\%$ for the compression moulded and $24 \pm 2\%$ for the sintered materials at 25 N). This is the range in which the material is behaving auxetically and the indentation resistance is enhanced. As the test load increases, the auxetic effect is gradually lost and the material behaves in a more plastic fashion until at the higher test loads, the auxetic material is the most plastic of those tested (i.e. at 250 N, the retained deformation for the auxetic material

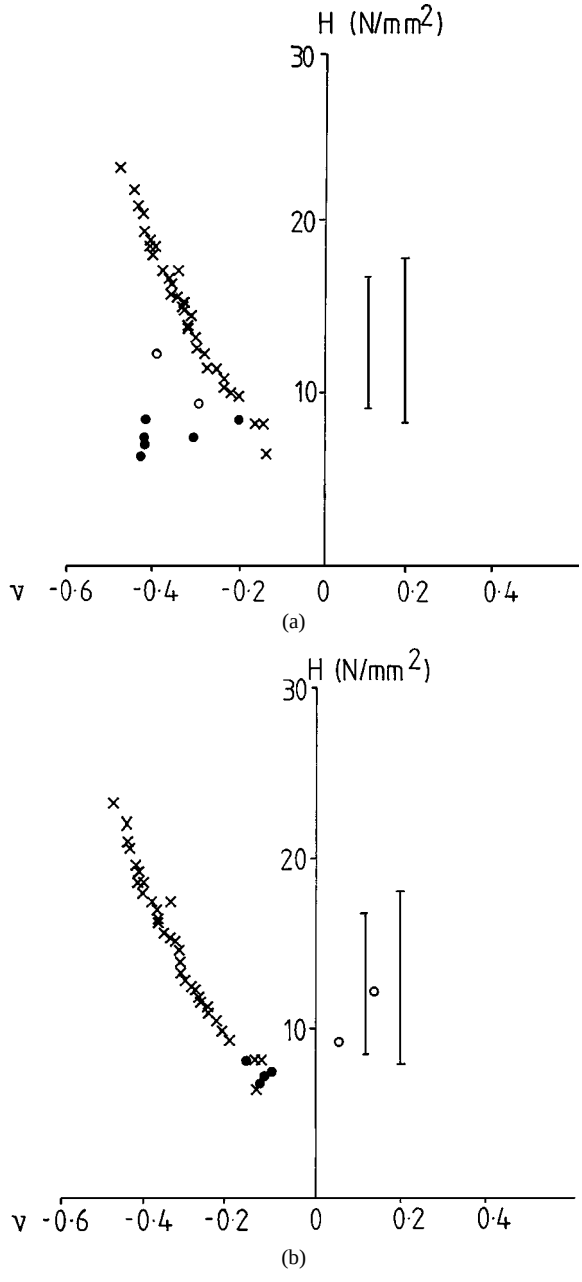

Figure 7 Graph of elastic indentation resistance (H_e against Poisson's ratio (ν_{rz}) at a test load of 25 N. (a) shows the test data analysed using one initial angle, $\alpha_0 = 20^\circ$ and (b) shows the test data where α_0 is allowed to vary for individual scattered points such that $\alpha_0 = 50^\circ$ or $\alpha_0 = -50^\circ$. Scatter is eliminated. Test data are represented by crosses for $\alpha_0 = 20^\circ$, filled circles for $\alpha_0 = 50^\circ$ and open circles for $\alpha_0 = -50^\circ$ so that the angles can be identified. This key also applies in Fig. 7a so that the scatter points are identified even though all data here is assigned $\alpha_0 = 20^\circ$. For comparison, the sintered and compression moulded data are also included as lines at $\nu = +0.11$ and $+0.2$ respectively.

is $37 \pm 1\%$ whereas it is $31 \pm 1\%$ for the compression moulded material and $33 \pm 2\%$ for the sintered material).

It should be noted that the sintered material behaves plastically even at low loads, having three times the retained deformation of the auxetic material and approximately twice that of the compression moulded material at 25 N. The possible reasons for this are considered in the next section.

Since polymeric materials show a complex viscoelastic behaviour, it was decided to observe the samples again after a period of 1 month (approximately 720 hours) to see if there had been any further viscoelastic recovery of the indents. It was expected that this would be the case since previous work by Lorenzo *et al.* [24] had shown that impressions produced in polyethylene by Vickers microindentations did not remain constant in shape but recovered with time. All three types of material were measured after the 1 month period to see if any differences could be observed between the auxetic, sintered and compression moulded materials. It was found that no impression could be observed in the sintered material which had been tested to loads of 15 N and 25 N but impressions could still be seen for specimens tested at loads of 50 N and above. For the compression moulded material, the lowest load applied to a specimen after which an impression remained after 1 month was 75 N and for the auxetic material, it was 100 N. This indicates that the auxetic material displays the most rapid viscoelastic creep response, with the material losing, effectively, all trace of the indent at loads of up to and including 75 N after 720 hours.

TABLE II The percentage instantaneous retained deformation for the sintered (S), compression moulded (CM) and auxetic (A) materials

Test load (N)	Percentage instantaneous retained deformation for		
	CM	S	A
15	7 ± 1	11 ± 3	5 ± 2
25	13 ± 2	24 ± 2	8 ± 2
50	21 ± 5	19 ± 1	22 ± 2
75	22 ± 5	27 ± 1	24 ± 1
100	17 ± 3	29 ± 1	28 ± 2
150	28 ± 2	30 ± 1	28 ± 3
200	32 ± 4	31 ± 2	33 ± 1
250	31 ± 1	33 ± 2	37 ± 1

5. Discussion

Before discussing the results of this study, the method and complexity of the analysis and modelling required to interpret the data should be commented on. Ideally, the Poisson's ratio of the material under test should be measured directly at all deformations instead of being predicted for the different values of H_e (albeit using the experimentally determined values of N, α_0, l, a and b). This issue is currently being addressed by conducting continuous strain history tests on auxetic and equivalent positive Poisson's ratio materials using video extensometry techniques.

The main finding from this work is that indentation resistance is enhanced in auxetic UHMWPE when compared with conventional UHMWPE under test loads of 10–100 N with a maximum increase of a factor of $\times 8$ from $\nu \approx 0$ to $\nu \approx -0.85$. It should also be noted that at the higher test loads (i.e. 150 N and 200 N), the indentation resistance of the auxetic materials might not be enhanced but it is at least equal to that of the sintered and compression moulded materials so even after the auxetic effect is lost, the indentation resistance does not decrease but rather becomes conventional.

The large variation seen in the range of indentation resistance values for the auxetic material can be attributed to microstructural variations and this is in itself borne

out by the fact that four initial angles are required to completely and comprehensively analyse and interpret the data. The initial angles required to describe fully the nodule-fibril microstructure are $\alpha_0 = +20^\circ$, $+50^\circ$, -20° and -50°, and use of these have allowed any scatter in the data to be accounted for (see Fig. 7a and b). The microstructural variations are an issue and obtaining homogeneity in all samples is one of the main aims of future work in the processing of auxetic, microporous polymers. Otherwise, all the properties of the material will vary along the specimen length, making every section effectively a different material.

The elastic/plastic/viscoelastic nature of the indentation response which has been characterised by the recovery of the indentation impression immediately after the test load was removed and after 720 hours (i.e. 1 month) was also investigated. The auxetic material proved to be the most elastic of the three materials at the two lower loads of 15 N and 25 N, with the sintered material being the most plastic. For example, at a test load of 25 N, the auxetic material retained only $8 \pm 2\%$ of its indentation depth after the load was removed whereas the sintered material retained $24 \pm 2\%$. This is an important finding as it points to the cooperative behaviour of the nodules and fibrils in the microstructure of the auxetic material being instrumental in its response to indentation rather than it being simply due to the closing up of the pores in the material. If the latter were the case, then the sintered material would behave exactly as the auxetic material does. However, the sintered material appears to be squashed under the indenter (see Fig. 8a). This is further underlined by the findings after 1 month. Even allowing for such a long recovery time, the impression remained clearly visible to the naked eye in sintered specimens which had been tested up to loads of only 50 N. This is the most plastic response seen.

The results from this study can be used, then, to suggest how the auxetic material reacts to indentation. The mechanism proposed must take account of the facts that the material is more difficult to indent the more auxetic it is and that the response is more elastic than that in both the sintered and compression moulded materials. This suggests that the material response is microstructural in nature and, from the differences in behaviour between the sintered and auxetic materials, is believed to be due to the fibrils. The mechanism proposed here involves the cooperative behaviour of the nodules and fibrils such that the fibrils pull the nodules under the indenter, causing a local densification of the microstructure (see Fig. 8b). The shaded circles in Fig. 8b represent the nodules (as did the shaded regions in Fig. 4) and the solid lines the interconnecting fibrils, as labelled. It is believed that the fibrils wrap around the nodules when the indenter is applied and further work is underway to observe this process in the straining stage of an SEM to verify if this is the case. Thus, the fibrils appear to disappear in Fig. 8b(ii) but are actually wrapped around the nodules, conforming to their shapes. This is the same type of effect seen when auxetic honeycomb structures are indented [25] which adds credence to the ideas expressed here.

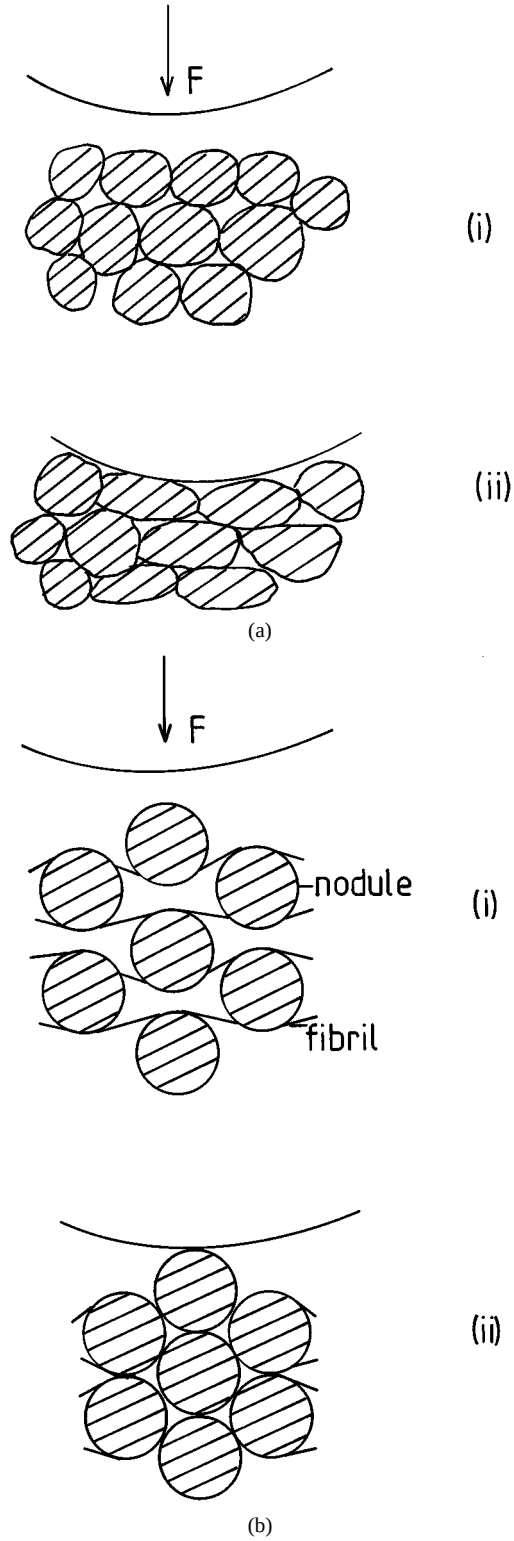

Figure 8 Schematic showing the proposed microstructural response for indentation of (a) sintered and (b) auxetic polymers. In each case, (i) represents the polymer before indentation and (ii) represents the polymer under indentation. The shaded circles represent the nodules.

If the indentation response is due to local densification under the indentor, then in the more open regions of the specimen, this would be achieved more easily due to the cooperative nature of the response of the nodules and fibrils, resulting in a material that is more difficult to indent. Then, on removal of the load, it is expected that the fibrils would unwrap and nodules would relax and return to close to their original positions. This would explain the much more elastic nature of the indentation

response for the auxetic material compared with the sintered material at low loads. Also, it would then be expected that further relaxation due to the viscoelastic response would take place over a period of time as the microstructure gradually returns to its initial state. This is also the case with much less permanent damage effected for the auxetic material than the sintered material characterised by the fact that no impression can be seen in samples that had been tested up to and including 75 N for the auxetic material whereas the lowest load investigated where recovery of the impression was complete for the sintered materials was only 25 N.

The auxetic material does become more plastic at the higher loads considered than the other two material types. The reason for this is that the nodules and fibrils are completely densified under the indenter and further loading in this state can only lead to plastic deformation of the microstructure.

6. Conclusion

The indentation resistance of auxetic UHMWPE is enhanced at low loads (i.e. up to 100 N when the strains imposed on the microstructure cause the auxetic effect to be lost) when compared to sintered and compression moulded UHMWPE.

It was found that the auxetic material was the most elastic at the lower test loads and was also had the most rapid viscoelastic response, which was assessed by re-examining the specimens after 1 month. The sintered material had the most plastic response and this has allowed a mechanism to be proposed explaining how the microstructure of the auxetic material reacts to indentation. This is proposed to take place by the local densification of the nodules caused by the fibrils under the indenter and not simply by the closing up of the pores in the material, which would mean that the sintered and auxetic materials would behave identically. Verification of this microstructural mechanism is continuing in current work.

Acknowledgements

The authors wish to acknowledge the financial support of BNFL (AF).

References

1. R. LAKES, *Science N.Y.* **235** (1987) 1038.
2. C. P. CHEN and R. S. LAKES, *J. Mat. Sci.* **26** (1991) 5397.
3. B. D. CADDOCK and K. E. EVANS, *J. Phys. D: Appl. Phys.* **22** (1989) 1877.
4. K. L. ALDERSON and K. E. EVANS, *Polymer* **33** (1992) 4435.
5. A. P. PICKLES, K. L. ALDERSON and K. E. EVANS, *Polym. Eng. and Sci.* **36**(5) (1996) 636.
6. J. P. DONOGHUE and K. E. EVANS, in Proc. ICCM8, Honolulu, 1991, edited by S. W. Tsai and G. S. Springer (SAMPE), Covina 2-K-1-10.
7. K. E. EVANS, I. J. HUTCHINSON, M. A. NKANSAH and S. C. RODGERS, *Nature* **353** (1991) 124.
8. K. E. EVANS, *Chem. Ind.* **20** (1990) 654.
9. R. LAKES, *Dev. Mech.* **14b** (1987) 758.
10. H. HERTZ, *J. Maths (Crelle J)* **92** (1881)
11. S. P. TIMOSHENKO and J. N. GOODIER, "Theory of Elasticity," 3rd ed. (McGraw Hill, New York 1970) p. 403.
12. R. S. LAKES and K. ELMS, *J. Comp. Mat.* **27**(12) (1993) 1193.
13. N. CHAN and K. E. EVANS, *J. Cellular Plastics* **35**(2) (1999) 130.
14. K. L. ALDERSON, A. P. PICKLES, P. J. NEALE and K. E. EVANS, *Acta Met. et Mat.* **42**(7) (1994) 2261.
15. Y. TIRUPATAIAH and G. SUNDARARAJAN, *Mat. Sci. and Eng.* **91** (1987) 169.
16. A. P. PICKLES, R. S. WEBBER, K. L. ALDERSON, P. J. NEALE and K. E. EVANS, *J. Mat. Sci.* **30** (1995) 4059.
17. K. L. ALDERSON, A. P. KETTLE, P. J. NEALE, A. P. PICKLES and K. E. EVANS, *J. Mat. Sci.* **30** (1995) 4069.
18. P. J. NEALE, A. P. PICKLES, K. L. ALDERSON and K. E. EVANS, *ibid.* **30** (1995) 4087.
19. Hoechst UK Ltd., Hoechst House, Salisbury Rd, Middlesex, TW4 6JH.
20. E. MURPHY, private communication.
21. R. J. CRAWFORD and G. STEPHENS, *Polymer Testing* **5** (1985) 113.
22. K. L. ALDERSON, A. ALDERSON and K. E. EVANS, *J. Strain Analysis for Eng. Design* **32**(3) (1997) 201.
23. D. TABOR, "The Hardness of Metals" (Oxford Univ. Press 1951) p. 44.
24. V. LORENZO, J. M. PERENA, J. G. FATOU, J. A. MENDEZ-MORALES and J. A. AZNAREZ, *J. Mat. Sci.* **23** (1988) 3168.
25. I. G. MASTERS, Ph.D. thesis, University of Liverpool, 1994.

Received 26 August, 1999
and accepted 14 February, 2000